"Gheorghe Asachi" Technical University of Iasi, Romania

COMPUTATIONAL FLUID DYNAMICS BASED MODELING
OF A LINEAR HEAT SOURCE

Raluca Teodosiu∗, Lidia Niculiţă, Cătălin Teodosiu

Faculty of Building Services and Equipment, Technical University of Civil Engineering
Lacul Tei Bvd., no. 122-124, Bucharest 020396 Romania

Abstract

In this paper, a study is conducted to assess the ability and the accuracy of a CFD approach concerning the behavior of a linear heat source positioned in a test room. Firstly, the main characteristics of our numerical model (mesh generation, turbulence model, near wall treatment, radiation model and boundary conditions) are presented after a briefly description of the test room taken into account. In addition, we show also the significance of these issues within our CFD approach. Furthermore, comparing the results obtained with those from experiments tests, the numerical model precision is evaluated. As a result, we notice a correctly plume description which allow us to achieve a proper general airflow prediction in the heated room (including thermal stratification and pollutant diffusion). On the contrary, we detect relatively important experimental – numerical differences regarding the heat transfer at walls. Therefore, the boundary layer description as well as the radiation model has to be improved. This must be correlated with the measurements precision in order to be able to achieve more complete and accurate experimental data.

Key words: buoyancy driven cavity, CFD - Computational Fluid Dynamics modeling, heat source, thermal plume

Received: February, 2014; Revised final: August, 2014; Accepted: August, 2014

1. Introduction

The CFD approach is a promising way to predict the air movement in a room and we observe nowadays that this technique is applied more and more in studies dealing with ventilation effectiveness (Kwon et al., 2011), indoor air quality (Shen et al., 2013) and thermal comfort (Catalina et al., 2009; Chiang et al., 2012). On the contrary, we can notice during the last decades that the zonal models (Allard and Inard, 1992; Megri and Haghighat, 2007; Song et al., 2008) were used in order to predict the thermal coupling between a radiator and a dwelling (thermal stratification, heat transfer, plume behavior) but due to hardware evolution, the CFD technique can be employed at the present in this important field, too.

Consequently, this paper brings elements in this field of research, the main objective of this work being the ability and the accuracy of a CFD model to study a heated room. The precision of such a numerical simulation is clarified by comparing the results achieved with those from experiments. Therefore we first present briefly the experimental set-up followed by the principal characteristics of our numerical model.

2. Experimental set-up

Our study is entirely based on the measurements presented in the analysis (Inard, 1988). The tests were carried out in a climatic test room ($3.1 \times 3.1 \times 2.5$ m³) in steady state conditions on one electric linear heat source. Succinctly, the configuration of this test room is the following (Fig. 1):
- a window (single glazed) situated in the front wall ("façade"). Its thickness is 1 cm and its thermal conductivity was considered 1 W/mK. This part of

---

∗ Author to whom all correspondence should be addressed: e-mail: ralucahohota@yahoo.com

the test room is in contact with ambient temperature (between –10°C and 40°C).

 - the other walls are in contact with environmental temperatures (between 20-25°C).

The electrical heat source was located near the front wall (see Fig. 2). It is formed by three elements, 1 m length each. Throughout the tests, the length and the heating capacity (power) were varied in order to establish the behavior of the linear heat source. It is worthwhile to mention that synchronized measurements of voltage and intensity for each element allowed knowing the total power of the system with a precision of ±0.5% (Inard, 1988).

This was correlated with the external temperature imposed at the front wall. The configurations studied here are presented below in Table 1.

Further, there were two kinds of measurements:

 - boundary conditions measurements type, namely surface temperature inside and outside the walls in order to find out the conductive rates and to determine too the radiative heat exchanges between walls as well as between these and the heat source. As a result, a network of 114 thermocouples (24 x 1 surface – "south" wall and 18 x 5 surfaces – other

walls) was employed for a good knowledge of the test room thermal state; the thermocouples were positioned in the surface layer of the outer and inner surfaces (in vis-à-vis) of each wall; the sensors used are type K (Chromel-Alumel) thermocouples (diameter 2 x 10^{-4} m and accuracy ±0.15ºC); in addition, platinum resistance thermometers (RTD sensors Pt 100 Ω, accuracy ±0.05ºC) were used to control the air temperature within the spaces adjoining the walls of the test cell.

 - field measurements (temperature and velocity) using an automatic device that moves the sensors over different planes in the test room. The instruments mounted on this device were omnidirectional hot-film transducers for air velocity (accuracy: ±3% of the selected full scale measurement) and type K (Chromel-Alumel) thermocouples (diameter 2 x 10^{-4} m and accuracy ±0.15ºC) for air temperature. This automatic device "transported" the sensors over the vertical median plane of the test room (perpendicular to the glass wall). The heat source plume region was specially examined in this plane. Fig. 3 shows the measurement points mesh above the linear heat source.
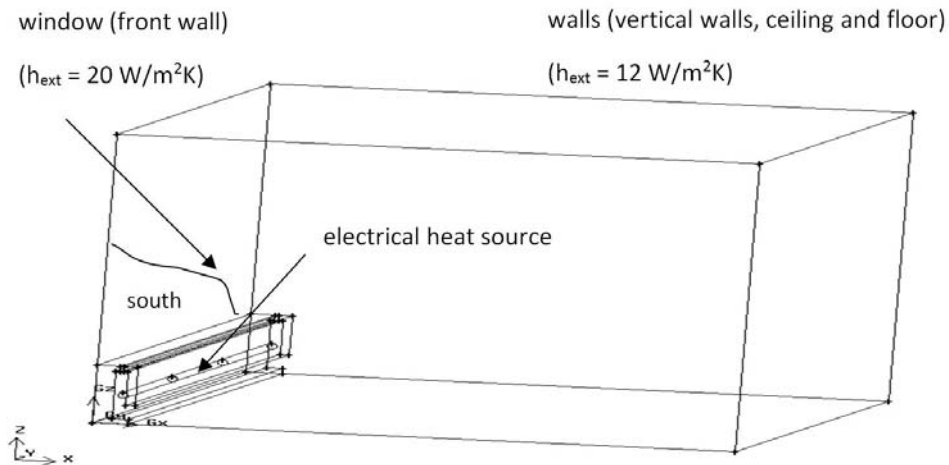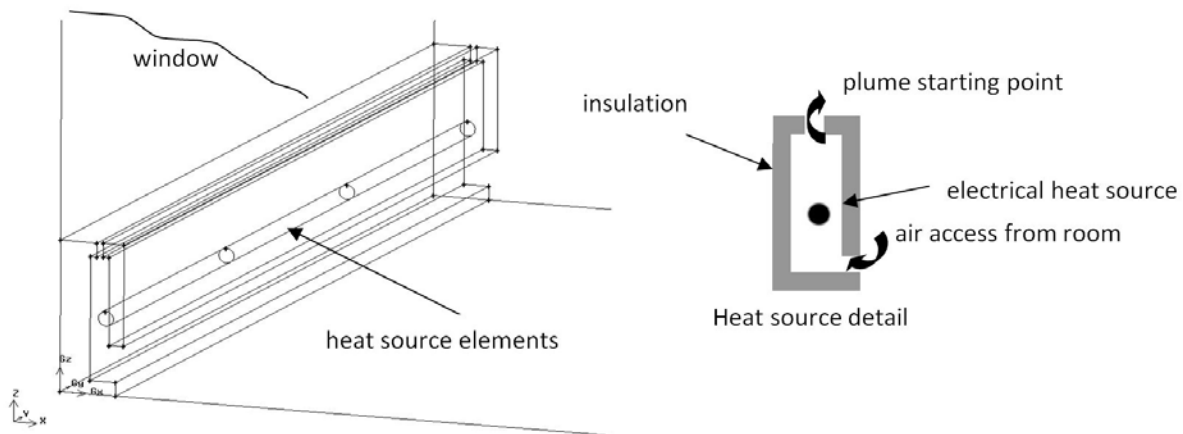
window (front wall)

(h_{ext} = 20 W/m²K)

walls (vertical walls, ceiling and floor)

(h_{ext} = 12 W/m²K)

electrical heat source

south

Fig. 1. Test room configuration

window

heat source elements

insulation

plume starting point

electrical heat source

air access from room

Heat source detail

Fig. 2. Electrical heat source location and detail

Table 1. Experimental test configurations

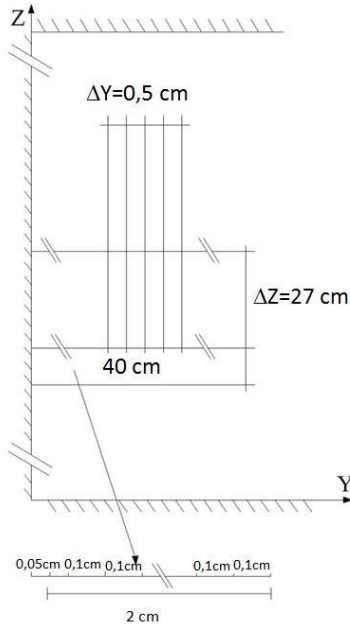| *Test*	*Heat source elements*	*Power (W)*	*Ambient temperature – front wall ($^\bullet C$)*
R1P2	1	810	1.4
R3P1	3	1159	-5.3

Fig. 3. Temperature and velocity measurements points in the heat source plume (Inard, 1988)

3. Numerical model

In this part of our work, we develop the principal features of our numerical model. In fact, we focus on its main elements that have a major impact on the simulations. Basically, the approach is based on a commercial CFD code, Fluent. This general-purpose code is a finite volume, Navier-Stokes solver (Fluent, 1998). We begin this section by the discretization of computational domain.

3.1. Mesh

The discretization of computational domain is achieved by means of an unstructured mesh. The grid contains tetrahedral elements obtained due to a mesh generation algorithm based on the Delaunay criterion. This meshing technique is by far, the most popular of the grid generation methods concerning the tetrahedral creation (Thompson et al., 1998). There are three reasons that justify our option regarding an unstructured grid:
 - first of all, the unstructured grid is ideally suited for the discretization of complicated geometrical domains. In our case, this allows us an exact description of electrical heat source tubes. This is an important issue, related to the setting of the proper volumetric heat generation rate for the heat source

(see the next section about the heat source computation).
 - besides, our flow field is a complex one, therefore there is no advantage to using a hexahedral (structured) mesh since the flow is not aligned with the mesh (the numerical diffusion is minimized if the flow tracks the shape of grid elements).
 - finally, another advantage of the unstructured mesh is that it allows us to refine without difficulty the grid based on geometric or numerical solution data. This property is very useful for the regions of the domain where strong flow gradients occur (boundary layers, plumes or jets). The grid in these zones can be refined without adding unnecessary cells in the other parts of the domain as classically happens in the structured grid approach.

Concerning the last mentioned benefit, this feature was applied in the plume area within our model in order to acquire a better discretization of this zone with intense gradients. As a result, we obtained more than 47000 cells in the vicinity of the heat source in comparison with 6000 finite volumes in the same zone before the mesh refinement (test R1P2).

It is worthwhile to mention that this technique has been successfully used for buoyancy driven cavities to reduce the numerical diffusion in recent studies (Ahanj et al., 2012; Shati et al., 2011).

3.2. Turbulence model

There are several considerations that influence the choice of turbulence model. The most important ones, which guide our selection too, consist in the accuracy and the simplicity of the turbulence model. Another important criterion in this choice is related to the demanded computational resources in the application of the turbulence model. Therefore, we employ in our study a revised k-ε turbulence model, the realizable k-ε model (Shih et al., 1995). This model answers fairly well at all the demands listed before. In fact, the standard k-ε model is till now by far the most widely used and validated of the classical models.

On the other hand, its extensive employment has made known too its weaknesses. Initial studies (Fluent, 1998) have shown that the realizable k-ε model reduces or even removes some of the k-ε model deficiencies. For instance, the spreading rate of both planar and round jets is more precisely predicted by the means of realizable k-ε model. Moreover, the superiority of the realizable k-ε model has been established too for flows including boundary layers under strong adverse pressure gradients, separation and recirculation (Hussain and Oosthuizen, 2012; Teodosiu et al., 2003). This version of the classical k-ε model contains a different model dissipation rate equation and eddy viscosity formulation. In fact, the eddy viscosity (μ_t) is

determined from the same equation as in other k-ε models (Eq. 1):

$$\mu_t = \rho C_\mu \frac{k^2}{\varepsilon} \qquad (1)$$

where: ρ represents the density; k and ε correspond to the turbulence fields: turbulent kinetic energy and its rate of dissipation, respectively.

The difference is that C_μ is no longer constant (0.09) as in the standard model. Its value is a function of the mean strain and rotation rates, as well as of the turbulence parameters, k and ε (Shih et al., 1995). This relationship makes vanish the overprediction of the eddy viscosity for flows with a high mean shear rate, deficiency identified in the case of the standard k-ε model.

In addition, the modeled transport equation for ε is to a certain extent different from those in the standard model. The differences and their physical and mathematical meanings are entirely exposed in (Fluent, 1998; Shih et al., 1995). Anyway, the purpose of these modifications is to obtain a more appropriate turbulence length scale.

3.3. Near wall treatment

Correct calculation of an enclosed turbulent flow is not possible without an adequate description of the flow in the near wall region. The turbulence model briefly described in the previous section is valid only for the flow far from walls (high Reynolds number). In order to deal with the near wall region, the classical CFD approach is based on logarithmic wall functions (Versteeg and Malalasekera, 1995). This technique allows important computational savings, as within this method, the near wall region is not resolved, it is instead linked via the wall functions.

Unfortunately, the wall functions were initially created for forced convection flows and their application is inappropriate for natural convection flows (Beausoleil-Morrison, 2000; Beghein, 1992). Subsequently, we employ another near wall model in our study (the two-layer zonal model), suited both for strong body forces and important three-dimensionality of boundary layer (in the region where the plume impinge the ceiling).

Basically, the two-layer approach (Fluent, 1998) separates the computational domain into a viscosity affected region (in the neighborhood of the wall) and a fully turbulent region. The demarcation between these two regions is founded on the turbulent Reynolds number (Re_y) – based on the normal distance from the wall at the cell. In the viscosity near-wall region ($Re_y < 200$), a one-equation model (only for the turbulent kinetic energy) is employed. For this reason, the dissipation rate of the turbulent kinetic energy ε is obtained algebraically by means of length scales. The complete expressions that determine the turbulent

viscosity and turbulent kinetic energy are given in (Fluent, 1998).

3.4. Radiation model

Due to high temperature established on the surface of the heat source, the radiation heat transfer has to be included in our simulations. The air is considered a nonparticipating media, despite of the fact that humid air contains water vapor which is an absorbing element in the infrared. This assumption has been used with satisfactory results in other similar studies (Tabarki and Mabrouk, 2012). In addition, all surfaces taken into account within the model (room walls and radiator faces) have the following properties: grey scattering surfaces (transmission and reflection).

There are a number of methods to compute the radiation heat transfer within CFD simulations: discrete transfer, P-1, Rosseland or discrete ordinates. Nevertheless, in configurations with concentrated heat sources, the discrete ordinates (DO) radiation model is the most appropriate (Gao, 2011; Ploskic and Holmberg, 2010). Moreover, the additional computational cost required by this radiation model is modest in comparison with the other radiation models. As a result, we make use of the DO method in our numerical model in order to predict the radiative fluxes. More precisely, the method used represents a conservative variant of the DO radiation model, the finite-volume scheme (Raithby and Chui, 1990). In effect, this approach solves a transport equation (analogue to those for the fluid flow and energy) for radiation intensity in the spatial coordinates (x, y, z).

The number of these transport equations is given by the number of discrete solid angles defined, angles associated with a fixed vector direction in the coordinate system (x, y, z). In our case, we employ two control angles for the polar and azimuthal angles in order to position the vector direction in space. These control angles define the discretization of each octant of the angular space. Based on the results achieved, concerning the radiation heat transfer (Table 3), this quite roughly angular discretization must be refined. Finally, the radiation field is determined once every 10 global (solution process) iterations.

3.5. Boundary conditions

In our computation, walls bound the domain all over thus the boundary conditions are supplied only for this type of frontier. First of all, the no-slip boundary condition is assured at walls.

Regarding the thermal boundary conditions at wall frontiers, we impose a convective heat transfer. As a result, we provide the external convective heat transfer coefficient (h_{ext}) and the external temperature (T_{ext}) in order to determine the heat flux to the wall (q) (Eq. 2):

$$q = h_f \left(T_W - T_f \right) + q_{rad} = h_{ext} \left(T_{ext} - T_W \right) \quad (2)$$

where: h_f represents the fluid side local heat transfer coefficient based on the local flow field conditions (turbulence level, temperature and velocity) and T_W is the wall surface temperature. In the same time, T_f correspond to the local fluid temperature and q_{rad} stands for the radiative heat flux to the wall from within the domain.

We employ for the external temperatures the values given by the experiments. On the other hand, the values imposed for the external heat transfer coefficient are relatively important seeing that at the front wall (window) the coefficient is 20 W/m^{2}K while for the other walls the value is 12 W/m^{2}K.

However, these values can be compared with the correlations given in the literature. Therefore, for an air velocity of 1 m/s at the external wall surface of the test room, this velocity being reported in (Inard, 1988), the convective heat transfer coefficient values based on the correlations given in (Roldan, 1985), vary from 6 to 17,1 W/m^{2}K. Hence, the values used in our study correspond rather to the upper part of this interval. Moreover, the higher value at the window was imposed in order to enforce a more important heat flux at the front wall, this being related to a more proper plume development.

3.6. Heat source computation

It is worthwhile to note that there are several potential strategies to deal with the CFD heat source description:
- uniform heat fluxes boundary conditions at heater faces.
- fixed temperature set for the whole heat source surface.
- simplified approach, the heat source is replaced by a convective heat source that does not represent an obstacle for the airflow.

Unfortunately, the first approach (based on fixed thermal flux on the heat source surface) leads to "a priori" imposition of heat exchanges while these deeply depend on the flow characteristics near the heat source. On the other hand, despite the good results that follow from the methods using fixed temperature set for the whole heat source surface (Sevilgen and Kilic, 2011; Shati et al., 2011) there is a lack of practical application because the heat source surface temperatures must be known. Moreover, these temperatures are not usually accessible for ordinary situations where there are not detailed experimental data. It must be said also that this approach "freezes" the surface temperature although these depend on local flow conditions in the vicinity of the heat source. Concerning the last method, based on purely convective heat source, we can not neglect the radiative heat transfers in our case.

Consequently, the heat source integration in our numerical model is performed by adding a term source in the energy balance equations of the cells representing the heat source discretization. More precisely, it is a volumetric heat generation rate (S_h) accordingly to the source power (Q) and its dimensions (V - volume), which is uniformly distributed throughout the heat source (Eq. 3):

$$S_h = \frac{Q}{V} \quad (3)$$

As a result, we have the following equation (solid medium with internal heat source, Poisson's equation), assuming homogenous and isotropic medium with a thermal conductivity λ independent of temperature (Eq. 4):

$$\frac{\partial}{\partial x_i} \left(\lambda \frac{\partial T}{\partial x_i} \right) + S_h = 0 \quad (4)$$

The correctness of this approach is demonstrated by the results obtained in term of test room thermal balance as well as those related to the plume dynamic and thermal fields over the heat source (see the next section regarding the achieved results).

4. Results and discussion

The computations show an accurate test room overall heat balance (Table 2).

Table 2. Room thermal balance

Test	Heat source power (W)	Overall room heat balance (W)
R1P2	810.0	811.8
R3P1	1159.0	1162.0

On the other hand, the results presented in Table 3 concerning the radiative heat fluxes at walls, provide relatively significant experimental – numerical differences (2-30%). This indicates the need to use a better angular discretization in the DO radiation model in order to improve the prediction of radiative heat exchange. This must be also correlated with the complex geometry in the adjacent area of the linear heat source (south wall). As a result, further work should be performed to better assess the sensitivity of results to the DO angular discretization.

In addition, the convective transfers at walls present the same differences. This means that the description of the boundary layers must be improved, too. Alternatively, we have to take into account also, the measurements precision (due to minor temperature variations on the walls, a correct flux evaluation is difficult to perform). Therefore, further experimental and numerical analyses are to be complete in order to obtain a more appropriate wall convective and radiative heat fluxes evaluation.

In contrast, the plume development is correctly taken into account within the numerical model. The experimental – numerical comparisons

show a good agreement both for the dynamic and thermal plume field at a sequence of elevations over the heat source.

This is exemplified at an altitude of 1 m (0.5 m over the plume starting point, Fig. 2) in the Figs. 4 and 5 for the test R1P2 and in the Figs. 6 and 7 for the test R3P1, respectively (the values reported in these graphics are obtained in the room median vertical plane).

In addition, the global convective flow generated in the enclosure by the thermal plume is well estimated by the numerical model developed here. This is exemplified by the temperature fields experimental – numerical comparisons in the test room (Fig. 8).

Table 3. Radiative heat transfers at walls

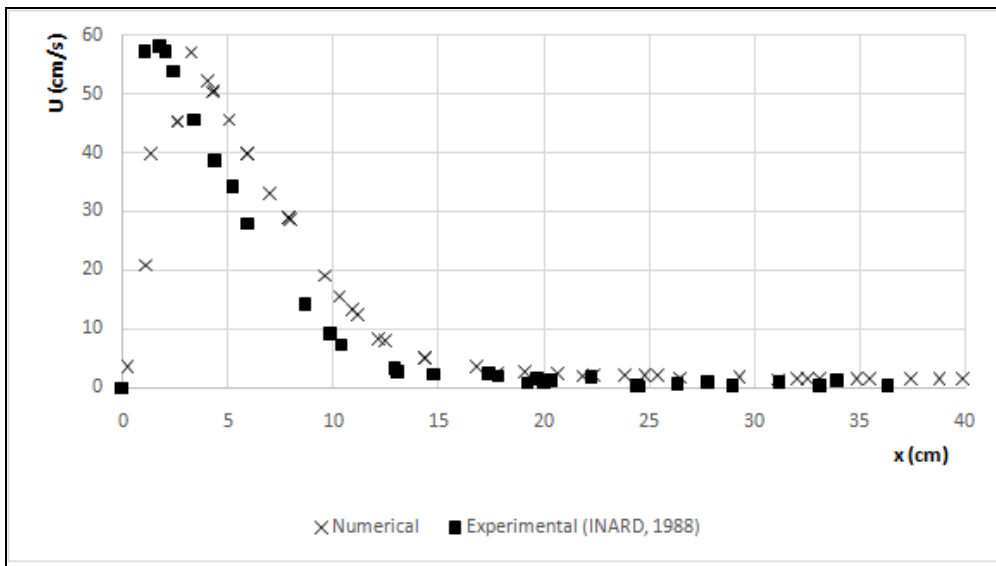| Wall	Radiative fluxes (W) - Test R1P2		Radiative fluxes (W) - Test R3P1	
	Experimental	*Numerical*	*Experimental*	*Numerical*
South	-391.4	-401.6	-359.7	-463.7
North	33.9	43.2	54.8	47.4
Ceiling	111.9	115.6	113.1	120.8
Floor	14.8	11.5	12.6	8.3
East	53.7	55.3	68.3	56.1
West	51.9	55.7	75.6	56.4

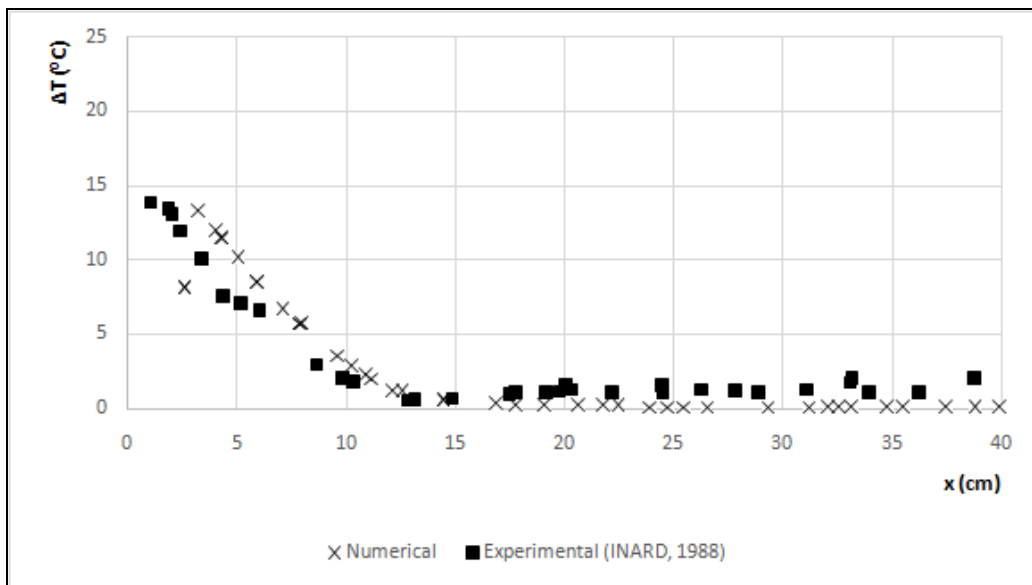**Fig. 4.** Velocity profile over the heat source (z = 1 m) – test R1P2

Fig. 5. Temperature profile over the heat source (z = 1 m) – test R1P2
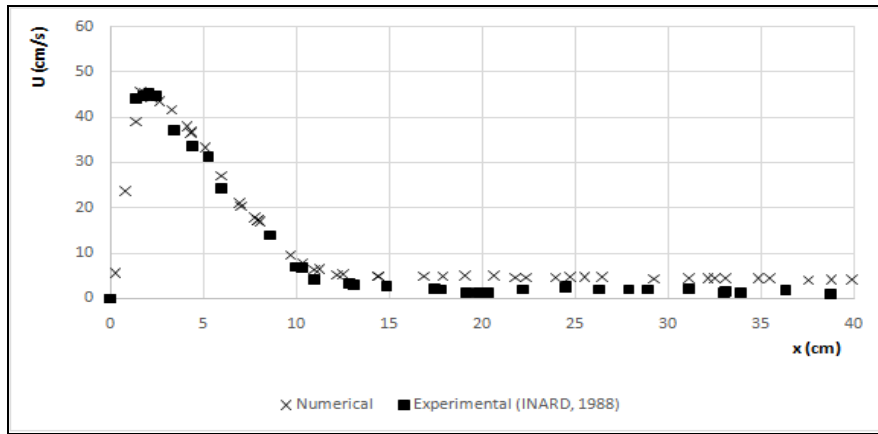
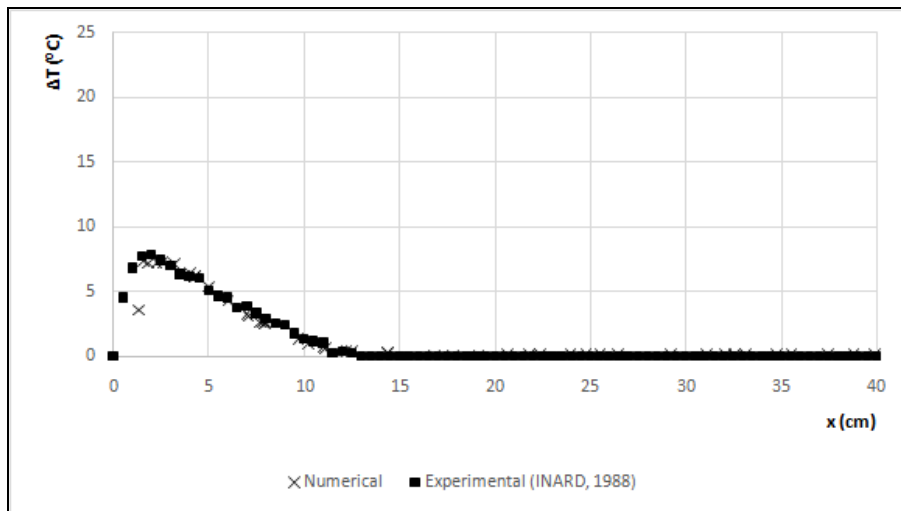**Fig. 6.** Velocity profile over the heat source (z = 1 m) – test R3P1

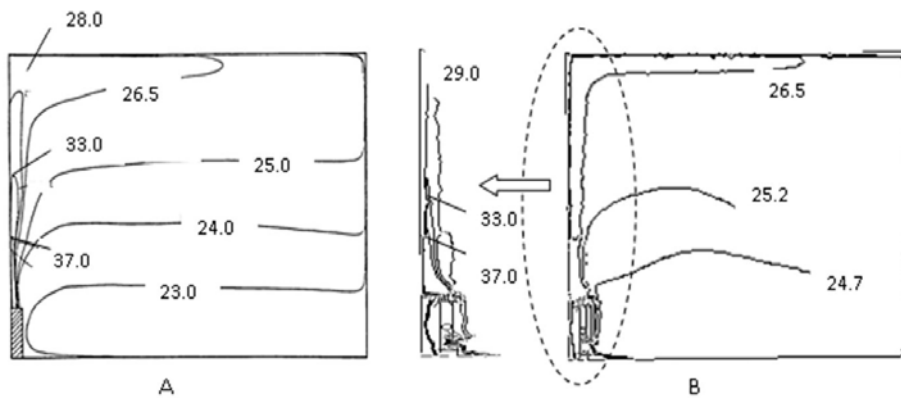**Fig. 7.** Temperature profile over the heat source (z = 1 m) – test R3P1

Fig. 8. Isothermal lines in the median vertical plane of the test room (°C), test R1P2.
A – experimental results; B – numerical results

On the other hand, it is known that the expansion of thermal plumes is influenced not only by the characteristics of the heat source (e.g. area, geometry, surface temperature) but also by the surroundings (e.g. presence of walls, furniture, or other airflows in their neighborhood) - (Zukowska et al., 2012). It is worthwhile to mention that all these factors can be naturally taken into account in CFD modeling.

5. Conclusions

The CFD numerical model is useful in applications concerning the airflow in heated rooms, the plume generated by a linear heat source being correctly characterized. This allows us to obtain reliable values concerning the heat flow as well as the air induction in the plume. This also generates an accurate airflow prediction within the entire heated

room (including thermal stratification and pollutant dispersion).

It is worthwhile to mention that this numerical model was applied for all the configurations studied in (Inard, 1988) concerning the linear heat source. In all cases, we remark the same characteristics of the numerical data: right plume development. Additionally, we must state that the data match better when there is only one heating element comparing with the three elements configurations. This means that the one element situation model (namely a decreased heat source area) is more straightforward to achieve.

On the other hand, the description of the thermal transfers at walls must be enhanced in order to achieve more proper results. These works should be also correlated with more complete and precise experimentations (e.g. infrared measurements). In addition, the external thermal boundary conditions (convective exchanges) must be also reconsidered to determine the exact computation sensitivity to this.

Finally, the simplified heat source approach presented here can be used for other localized sources of heat at floor level that differ in power, heat emission mode (convection or radiation), shape or size.

Acknowledgement

References

Ahanj M.D., Rahimi M., Alsairafi A.A., (2012), CFD modeling of a radiant tube heater, *International Communications in Heat and Mass Transfer*, **39**, 432-438.

Allard F., Inard C., (1992), *Natural and mixed convection in rooms: Prediction of thermal stratification and heat transfer by zonal models*, Proc. of the International Symposium on Room Air Convection and Ventilation Effectiveness, Tokyo, Japan.

Beausoleil-Morrison I., (2000), *The adaptive coupling of heat and air flow modelling within dynamic whole-building simulation*, PhD. Thesis, University of Strathclyde, Glasgow, UK.

Beghein C., (1992), *Contribution to the numerical study of thermosolutal natural convection in a cavity. Application of pollutant diffusion in rooms* (in French), PhD Thesis, INSA Lyon, France.

Catalina T., Virgone J., Kuznik F., (2009), Evaluation of thermal comfort using combined CFD and experimentation study in a test room equipped with a cooling ceiling, *Building and Environment*, **44**, 1740-1750.

Chiang W.H., Wang C.Y., Huang J.S., (2012), Evaluation of cooling ceiling and mechanical ventilation systems on thermal comfort using CFD study in an office for subtropical region, *Building and Environment*, **48**, 113-127.

Fluent, (1998), *Fluent User's Guide*, Fluent Inc, Lebanon (NH), USA.

Gao R., Li A., Zhang O., Zhang H., (2011), Comparison of indoor air temperatures of different under-floor heating pipe layouts, *Energy Conversion and Management*, **52**, 1295-1304.

Hussain S., Oosthuizen P.H., (2012), Validation of numerical modeling of conditions in an atrium space with a hybrid ventilation system, *Building and Environment*, **52**, 152-161.

Inard C., (1988), *Contribution to the study of the thermal coupling of a heat emitter with a room* (in French), PhD Thesis, INSA Lyon, France.

Kwon K.S., Lee I.B., Han H.T., Shin C.Y., Hwang H.S., et al., (2011), Analysing ventilation efficiency in a test chamber using age-of-air concept and CFD technology, *Biosystems Engineering*, **110**, 421-433.

Megri A.C., Haghighat F., (2007), Zonal Modeling for Simulating Indoor Environment of Buildings: Review Recent Developments and Applications, *HVAC&R Research*, **13**, 887-905.

Ploskic A., Holmberg S., (2010), Heat emission from thermal skirting boards, *Building and Environment*, **45**, 1123-1133.

Raithby G.D., Chui E.H., (1990), A finite volume method for predicting a radiant heat transfer in enclosures with participating media, Journal of Heat Transfer, 112, 415-423.

Roldan A., (1985), *Thermo-aeraulic study of building envelopes* (in French), PhD Thesis, INSA Lyon, France.

Sevilgen G., Kilic M., (2011), Numerical analysis of air flow, heat transfer, moisture transport and thermal comfort in a room heated by two-panel radiators, *Energy and Buildings*, **43**, 137-146.

Shati A.K.A, Blakey S.G., Beck S.B.M, (2011), The effect of surface roughness and emissivity on radiator output, *Energy and Buildings*, **43**, 400-406.

Shen C., Gao N., Wang T., (2013), CFD study on the transmission of indoor pollutants under personalized ventilation, *Building and Environment*, **63**, 69-78.

Shih T.H., Liou W.W., Shabbir A., Yang Z., Zhu J., (1995), A new k-ε eddy viscosity model for high Reynolds number turbulent flows, Computers Fluids, 24, 227-238.

Song F., Zhao B., Yang X., Jiang Y., Gopal V., et al., (2008), A new approach on zonal modeling of indoor environment with mechanical ventilation, *Building and Environment*, **43**, 278-286.

Tabarki M., Mabrouk S.B., (2012), The coupling in transient regime between the modelings of thermal and mass transfers inside a heated room and its radiator, *Heat Mass Transfer*, **48**, 1889-1901.

Teodosiu C., Rusaouen G., Hohotă R., (2003), Influence of boundary conditions uncertainties on the simulation of ventilated enclosures, *Numerical Heat Transfer, Part A: Applications – An International Journal of Computation and Methodology*, **44**, 483-504.

Thompson J.F., Soni B., Weatherrill N.P., (1998), *Handbook of Grid Generation*, CRC Press, Boca Raton (FL), USA.

Versteeg H.K., Malalasekera W., (1995), *An Introduction to Computational Fluid Dynamics: the Finite Volume Method*, Longman Scientific & Technical, Essex, UK.

Zukowska D., Melikov A., Popiolek Z., (2012), Impact of geometry of a sedentary occupant simulator on the generated thermal plume: Experimental investigation, *HVAC&R Research*, **18**, 795-811.